
ON THE LIPSCHITZ CONSTANT OF DEEP NETWORKS AND DOUBLE DESCENT

Matteo Gamba*
KTH
Sweden
mgamba@kth.se

Hossein Azizpour
KTH
Sweden
azizpour@kth.se

Mårten Björkman
KTH
Sweden
celle@kth.se

ABSTRACT

Existing bounds on the generalization error of deep networks assume some form of smooth or bounded dependence on the input variable, falling short of investigating the mechanisms controlling such factors in practice. In this work, we present an extensive experimental study of the empirical Lipschitz constant of deep networks undergoing double descent, and highlight non-monotonic trends strongly correlating with the test error. Building a connection between parameter-space and input-space gradients for SGD around a critical point, we isolate two important factors – namely loss landscape curvature and distance of parameters from initialization – respectively controlling optimization dynamics around a critical point and bounding model function complexity, even beyond the training data. Our study presents novel insights on implicit regularization via overparameterization, and effective model complexity for networks trained in practice.

1 Introduction

A longstanding question towards understanding the remarkable generalization ability of deep networks is characterizing the hypothesis class of models *trained in practice* (Hanin & Rolnick, 2019b; Novak et al., 2018). Indeed, finding a parameterization that accurately describes the class of generalizing trained networks could shed light on the mechanisms controlling model complexity (Neyshabur et al., 2015a,b).

At present, for a target network topology, constraints on its hypothesis class have been derived from postulated assumptions on the training data (Kawaguchi et al., 2022; Wei & Ma, 2019), loss margins (Bartlett et al., 2017), model architecture (Hanin & Rolnick, 2019b,a) as well as global optima (Ma & Ying, 2021). Particularly, many existing bounds on the generalization error of deep networks assume bounded dependence of the model function on the input variable, chiefly via uniformly bounded Lipschitz constant (Kawaguchi et al., 2022; Ma & Ying, 2021; Wei & Ma, 2019; Nagarajan & Kolter, 2018; Bartlett et al., 2017).

While such assumption may seem appealing for representing a well-behaved model function for fixed architectures, this view is at odds with the double descent phenomenon (Belkin et al., 2019; Geiger et al., 2019) – whereupon the test error depends non-monotonically on model size – which has been connected to smooth interpolation of training data (Gamba et al., 2022b; Bartlett et al., 2020; Belkin et al., 2018).

Hence, a natural question is *whether uniform upper bounds on the Lipschitz constant provide a faithful representation of the hypothesis class of networks trained in practice*.

Contributions In this work, (1) we present an empirical investigation of input-space smoothness of deep networks through their Lipschitz constant estimated on the training data, as model size varies; (2) we observe non-monotonic trends for the Lipschitz constant, showing strong correlation with double descent; (3) we establish a theoretical connection between the observed trends and parameter-space dynamics of SGD in terms of fundamental operators and quantities; (4) we present several correlates of double descent, providing insights on the hypothesis class of networks trained in practice and their effective complexity.

*Corresponding author.

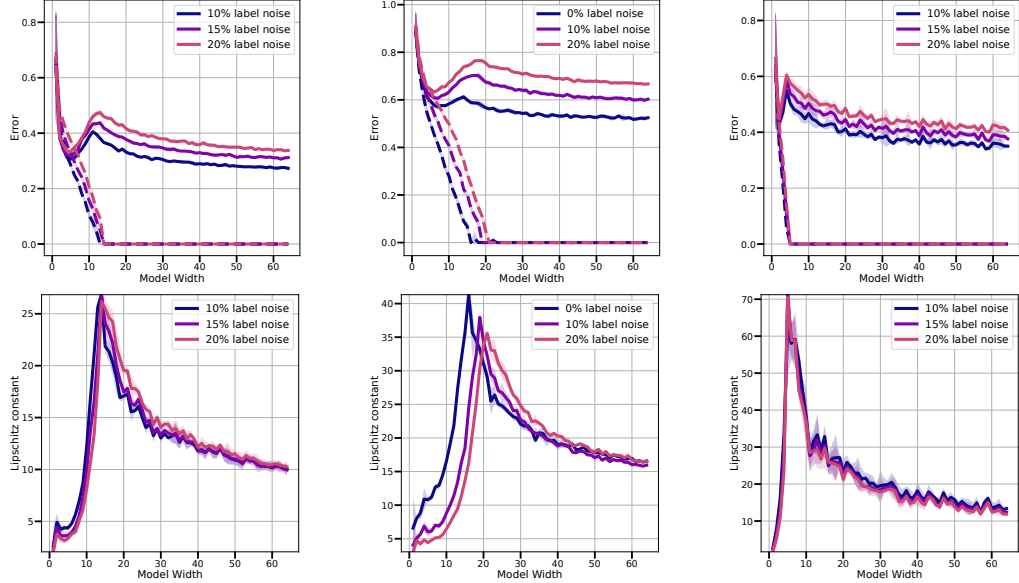


Figure 1: (Top) **Train error** (dashed) and **test error** (solid) for our experimental setting, with the test error undergoing double descent as model size increases. (Left to right) ConvNets trained on CIFAR-10 (left) and CIFAR-100 (middle), and ResNets trained on CIFAR-10 (right). (Bottom) **Empirical Lipschitz constant** for the same models. For each setting, the Lipschitz depends non-monotonically on model size, strongly correlating with double descent. This finding questions the utility and validity of uniformly bounded Lipschitz assumptions in representing the hypothesis class of trained networks.

Outline of the Paper Section 2 describes our experimental setup. Section 3 presents our main results, and connects the Lipschitz constant with parameter-space curvature of the loss landscape and model function. Section 4 discusses broader implications of our results. Finally, section 5 discusses our findings in connection to related works.

2 Experimental Details

We study the empirical Lipschitz constant of trained networks under double descent, when model size is controlled by network width. We reproduce the double descent curves of the test error (Belkin et al., 2019) by training a family of ConvNets and ResNet18s (He et al., 2015) on the CIFAR datasets (Krizhevsky et al., 2009) with up to 20% training labels randomly perturbed. Following Nakkiran et al. (2019), we control model size by increasing the number of learned feature maps ω of each convolutional stage in both model families, following the progression $[\omega, 2\omega, 4\omega, 8\omega]$, for $\omega = 1, \dots, 64$. To isolate the role of overparameterization, we remove potential confounders from the optimization process by training all networks with crossentropy loss and SGD with momentum and fixed learning rate, without any explicit regularization (full details in appendix B).

Figure 1 (top) shows the double descent curve for the test error for our experimental setting, with the test error showing the classic U-shaped curve for small models, and a second descent as the degree of parameterization increases further. By disabling explicit regularizers, we ensure that improvement in test error for large models is promoted by overparameterization rather than explicit regularization. Hereafter, we denote with *interpolation threshold* the smallest model width that perfectly classifies the training data.

3 Input-Smoothness Follows Double Descent

We begin by studying the empirical Lipschitz constant of piece-wise linear networks in section 3.1. Section 3.2 presents our main empirical finding, which we theoretically connect to parameter-space gradients in section 3.3. Finally, section 3.4 presents novel bounds on the empirical Lipschitz constant, that capture double descent in practice.

3.1 Preliminaries

We consider feed-forward networks $\mathbf{f}(\mathbf{x}, \boldsymbol{\theta}) : \mathbb{R}^d \times \mathbb{R}^p \rightarrow \mathbb{R}^K$, composing L affine layers with the continuous piece-wise linear activation $\text{ReLU } \phi(x) = \max\{0, x\}$, interpreted as functions $\mathbf{f}(\mathbf{x}, \boldsymbol{\theta}) = \boldsymbol{\theta}^L \phi(\boldsymbol{\theta}^{L-1} \phi(\dots \phi(\boldsymbol{\theta}^1 \mathbf{x} + \mathbf{b}^1)) + \mathbf{b}^{L-1}) + \mathbf{b}^L$, where $\boldsymbol{\theta} = (\text{vec}(\boldsymbol{\theta}^1), \dots, \text{vec}(\boldsymbol{\theta}^L)) \in \mathbb{R}^p$ represents the vectorized model parameter and $\mathbf{x} \in \mathbb{R}^d$ the input to the network.

For each fixed value of $\boldsymbol{\theta}$, $\mathbf{f}_\boldsymbol{\theta} : \mathbb{R}^d \rightarrow \mathbb{R}^K$ corresponds to a fixed hypothesis in the space \mathcal{H} of all functions expressible by the network architecture. Each model function $\mathbf{f}_\boldsymbol{\theta}$ is itself continuous piece-wise linear, and partitions its input space into convex polytopes known as activation regions (Raghu et al., 2017; Montufar et al., 2014), on each of which a linear function is computed. By piece-wise linearity, one can write

$$\mathbf{f}_\boldsymbol{\theta}(\mathbf{x}) = \sum_{\epsilon} \mathbb{1}_\epsilon(\mathbf{x}) \boldsymbol{\theta}_\epsilon \mathbf{x} + \mathbf{b}_\epsilon \quad (1)$$

where the indicator function selects the activation region according to \mathbf{x} , and $\boldsymbol{\theta}_\epsilon$ represents conditioning the factorization $\boldsymbol{\theta}_\epsilon := \prod_{\ell=1}^L \text{diag}(\phi_\mathbf{x}^\ell) \boldsymbol{\theta}^\ell$ by the binary activation pattern $\phi_\mathbf{x}^\ell$ of each ReLU according to the preactivation of the corresponding layer ℓ , dependent on the input \mathbf{x} to the network². Particularly, for an input $\bar{\mathbf{x}} \in \mathbb{R}^d$, evaluating the Jacobian $\nabla_{\mathbf{x}} \mathbf{f}_\boldsymbol{\theta}$ at $\bar{\mathbf{x}}$ yields $\boldsymbol{\theta}_\epsilon$, i.e. the linear function computed by $\mathbf{f}_\boldsymbol{\theta}$ on the activation region ϵ containing $\bar{\mathbf{x}}$. Hence, given a dataset $\mathcal{D} = \{(\mathbf{x}_n, y_n)\}_{n=1}^N$, the empirical Lipschitz of $\mathbf{f}_\boldsymbol{\theta}$ on \mathcal{D} can be estimated by computing the expected operator norm³

$$(\mathbb{E}_{\mathcal{D}} \|\nabla_{\mathbf{x}} \mathbf{f}_\boldsymbol{\theta}\|_2^2)^{\frac{1}{2}} := \left(\frac{1}{N} \sum_{n=1}^N \sup_{\mathbf{x}: \|\mathbf{x}\| \neq 0} \frac{\|\boldsymbol{\theta}_{\epsilon_n} \mathbf{x}\|_2^2}{\|\mathbf{x}\|_2^2} \right)^{\frac{1}{2}} \quad (2)$$

representing the expected largest change propagated by the function on activation regions covering \mathcal{D} , and can be thought of as a measure of scale of $\mathbf{f}_\boldsymbol{\theta}$. Appendix D outlines a procedure for estimating the operator norm in practice.

3.2 Input Smoothness of Piece-wise Linear Networks

Next, we compute Equation 2 for deep networks trained in practice. Figure 1 (bottom) presents our main result: *the empirical Lipschitz constant of deep networks is non-monotonic in model size, increasing until the interpolation threshold, and then decreasing afterward, strongly correlating with the test error.*

The empirical Lipschitz also correlates with hardness of the learning task, with interpolation threshold shifting towards larger models as label noise increases. The observed trends are consistent across all considered architectures, datasets, and noise settings.

This finding sheds light on the effective complexity of trained networks in relation to model size, contradicting the view of uniformly upper bounded Lipschitz constant adopted in many theoretical works (Kawaguchi et al., 2022; Ma & Ying, 2021; Wei & Ma, 2019; Nagarajan & Kolter, 2018; Bartlett et al., 2017), which miss the observed non-monotonicity, by taking the Lipschitz as a uniform constant.

The observed trends highlight a strong correlation between increased relative smoothness of the model function and its generalization ability, as well as dependency of the phenomenon on model size. It is important to note that the measure is computed exclusively on *training data*, and exhibits non-monotonic behaviour despite the training loss being monotonically decreasing with model size.

With the main message of the paper established, in the following sections we draw formal connections between the empirical Lipschitz and parameter-space regularity, and finally present and discuss further observations that offer deeper insights on model complexity and double descent.

3.3 Connection to Parameter-Space Dynamics

In this section, we connect input-space and parameter-space dynamics of SGD. We defer all proofs to appendix F. Let $\mathbf{x}^\ell = \phi(\boldsymbol{\theta}^\ell \mathbf{x}^{\ell-1} + \mathbf{b}^\ell)$ denote the output of the ℓ -th layer, for $\ell = 1, \dots, L$, with $\mathbf{x}^0 = \mathbf{x} \in \mathbb{R}^d$. We begin by noting that linear layers enjoy a duality between their input and parameters, for which $\frac{\partial \mathbf{x}^\ell}{\partial \mathbf{x}^{\ell-1}} \mathbf{x}^{\ell-1}{}^T = \boldsymbol{\theta}^{\ell T} \frac{\partial \mathbf{x}^\ell}{\partial \boldsymbol{\theta}^\ell}$, which implies the following statement.

²A similar conditioning is applied to compute the bias term \mathbf{b}_ϵ .

³The dependency of $\boldsymbol{\theta}_\epsilon$ from each sample \mathbf{x}_n is denoted by the activation region index ϵ_n .

Theorem 1. Let \mathbf{f} denote a neural network with a least one hidden layer, with $\|\theta^1\| > 0$ and arbitrary weights $\theta^2, \dots, \theta^L$. Let $x_{\min} := \min_{\mathbf{x}_n \in \mathcal{D}} \|\mathbf{x}_n\|_2$. Then, parameter-space gradients bound input-space gradients of \mathbf{f} from above:

$$\frac{x_{\min}^2}{\|\theta^1\|_2^2} \mathbb{E}_{\mathcal{D}} \|\nabla_{\mathbf{x}} \mathbf{f}\|_2^2 \leq \mathbb{E}_{\mathcal{D}} \|\nabla_{\theta} \mathbf{f}\|_2^2. \quad (3)$$

Crucially, the bound highlights the implicit regularization effect of parameter-space gradients on input-space gradients, by regularizing the empirical Lipschitz of \mathbf{f}_{θ} on the training data. Section 4 discusses implications beyond training data.

We note that, while an analogous bound was first observed by Ma & Ying (2021) (Theorem 3), the authors propose a uniform bound $\mathbb{E}_{\mathcal{D}} \|\nabla_{\theta} \mathbf{f}\| \leq \alpha p$ that linearly increases with the number of model parameters p , with constant α depending on learning rate and batch size.

In contrast, we study the bound in connection to double descent, as p varies with network width. Specifically, in section 3.4 we provide an upper bound to Theorem 1 that captures double descent in practical settings.

Implications Interestingly, by recalling that $\nabla_{\mathbf{x}} \mathbf{f}_{\theta} = \prod_{l=1}^L \text{diag}(\phi_{\mathbf{x}}^l) \theta^l$, the bound in Theorem 1 controls the expected growth of all layers save for θ^1 . This interpretation is well aligned with recent evidence showing that the scale of initialization of the first layer affects the magnitude of the parameter-space gradients, and may prevent an interpolating network from generalizing to test data (Mehta et al., 2020). Hence, the bound highlights the importance of carefully designed weight initialization schemes, as typically employed in practice (Arpit et al., 2019; He et al., 2015; Glorot & Bengio, 2010). We refer the reader to Mehta et al. (2020) for a detailed discussion on the problem.

Finally, for exponential losses $\mathcal{L}(\theta, \mathbf{x}, \mathbf{y})$ like crossentropy and mean squared error, an immediate corollary follows.

Corollary 1. Consider the composition of a loss function \mathcal{L} with a neural network \mathbf{f} with a least one hidden layer, with $\|\theta^1\| > 0$ and arbitrary weights $\theta^2, \dots, \theta^L$. Then,

$$\frac{x_{\min}^2}{\|\theta^1\|_2^2} \mathbb{E}_{\mathcal{D}} \|\nabla_{\mathbf{x}} \mathcal{L}\|_2^2 \leq \mathbb{E}_{\mathcal{D}} \|\nabla_{\theta} \mathcal{L}\|_2^2. \quad (4)$$

In the following, building on Corollary 1, we draw an explicit connection between $\|\nabla_{\mathbf{x}} \mathcal{L}\|_2$ and the parameter-space geometry of loss landscape.

3.4 Connection to Parameter-Space Curvature

In order to better elucidate the implicit regularization effect in Equations 3 and 4, we consider the dynamics of SGD in proximity of a minimum $\theta^* \in \mathbb{R}^p$ of the loss \mathcal{L} . We adopt a linear stability perspective (Hosoe & Hagiwara, 2022; Wu & Ma, 2018), and approximate the loss in a neighbourhood of θ^* via a second-order Taylor expansion

$$\mathbb{E}_{\mathcal{D}} \mathcal{L}(\theta, \mathbf{x}, y) = \frac{1}{2} (\theta - \theta^*)^T H(\theta - \theta^*) + o(\|\theta - \theta^*\|^3) \quad (5)$$

where the first order term vanishes at the critical point θ^* , as does the zeroth order term for interpolating models, and H represents the expected Hessian of the training loss.

In general, SGD with discrete learning rate is known to fluctuate around critical points due to stochastic noise (Mori et al., 2022; Liu et al., 2021). To study Theorem 1 in relationship to the dynamics of SGD around θ^* , we need to account for such phenomenon. In the next result, we adopt the noise model recently proposed by Ziyin et al. (2022),

to derive upper bounds on the empirical Lipschitz, focusing on the mean squared error $\mathcal{L} = \frac{1}{2N} \sum_{n=1}^N (f_{\theta}(\mathbf{x}_n) - y_n)^2$.

Theorem 2. Let θ^* be a critical point for the loss $\mathcal{L}(\theta, \mathbf{x}, y)$ on \mathcal{D} . Let \mathbf{f}_{θ} denote a neural network with at least one hidden layer, with $\|\theta^1\| > 0$. Then,

$$\frac{x_{\min}^2}{\|\theta^1\|_2^2} \mathbb{E}_{\mathcal{D}} \|\nabla_{\mathbf{x}} \mathcal{L}\|_2^2 \leq 2\mathcal{L}_{\max}(\theta) \Delta(\mathcal{L}(\theta)) + o(\mathcal{L}(\theta)) \quad (6)$$

with $\Delta(\mathcal{L}(\theta)) := \text{tr}(H)$ denoting the Laplace operator, $H := \mathbb{E}_{\mathcal{D}} \left[\frac{\partial^2 \mathcal{L}}{\partial \theta \partial \theta^T} \right]$ denoting the expected parameter-space Hessian of \mathcal{L} , and $\mathcal{L}_{\max}(\theta) := \max_{(\mathbf{x}_n, y_n) \in \mathcal{D}} \mathcal{L}(\theta, \mathbf{x}_n, y_n)$.

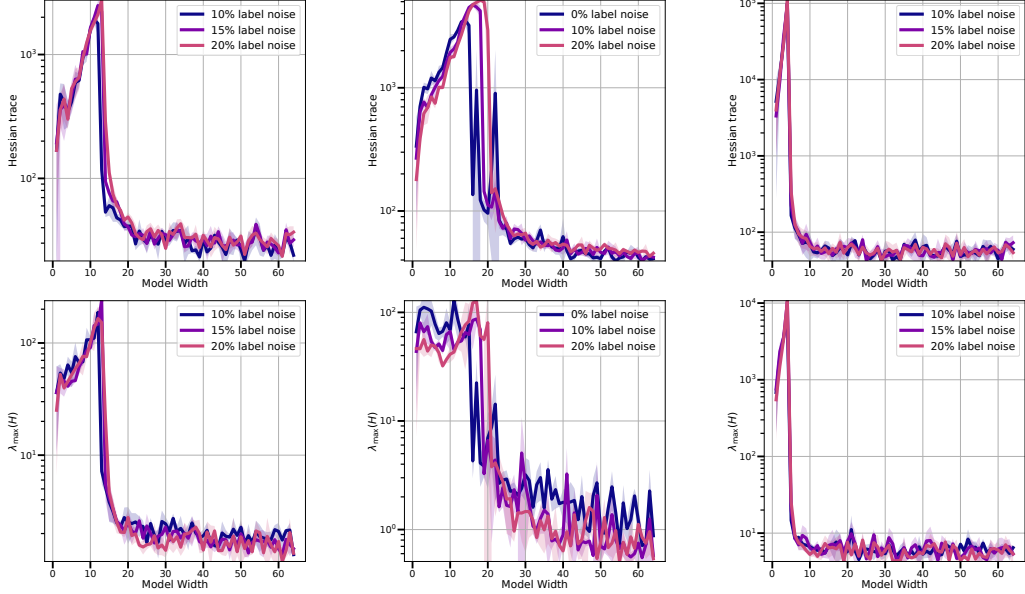


Figure 2: (Top) **Mean loss curvature** (Hessian trace) in parameter space. (Bottom) **Maximum curvature** for the loss in parameter space. From left to right: ConvNets trained on CIFAR-10 (left), CIFAR-100 (middle) and ResNets trained on CIFAR-10 (right). In all settings, mean and maximum parameter-space curvature strongly correlate with double descent, peaking at the interpolation threshold, and highlighting a nonlinear dependence on network width. All values are reported in log- y scale to better separate models in the interpolating regime.

Theorem 2 links network function regularity to the landscape of parameter space, via mean curvature $\Delta(H)$ of the loss in a neighbourhood of θ^* .

Figure 2 shows mean curvature of the loss landscape (top), as well as the largest loss Hessian eigenvalue $\lambda_{\max}(H)$ (bottom) estimated in parameter space for our experimental setup (see appendix D for algorithmic details). Both mean and maximum curvature closely match the model functions' Lipschitz constant as model width increases, peaking near the interpolation threshold and decreasing afterward. This substantiates our bound in Equation 6, and provides a characterization of the empirical Lipschitz constant in terms of fundamental quantities in parameter space (Hessian trace and λ_{\max}), which themselves capture double descent.

Fluctuation due to Stochastic Noise In proximity of a critical point θ^* , it is possible to derive linear stability conditions of Equation 6. We start by noting that, at each iteration t , the update rule of SGD with momentum μ , batch size B , and learning rate η , is given by

$$\begin{cases} \theta_{t+1} &= \theta_t - \eta \mathbf{g}_t \\ \mathbf{g}_t &= \mu \mathbf{g}_{t-1} + \frac{1}{B} \sum_{b=1}^B \nabla_{\theta} \mathcal{L}(\theta_{t-1}, \mathbf{x}_{\xi_b}, y_{\xi_b}) \end{cases} \quad (7)$$

with the random variables $\xi = (\xi_1, \dots, \xi_B)$ representing sampling of mini-batches. At step t , the stochastic noise ϵ_t of SGD is given by

$$\epsilon_t = \frac{1}{B} \sum_{b=1}^B \nabla_{\theta} \mathcal{L}(\theta_t, \mathbf{x}_{\xi_b}, y_{\xi_b}) - \mathbb{E}_{\xi} \nabla_{\theta} \mathcal{L}(\theta_t) \quad (8)$$

dependent both on the current parameter θ_t and ξ_t (Ziyin et al., 2022; Mori et al., 2022). Importantly, the noise covariance $C = \mathbb{E}_{\xi} [\epsilon_t \epsilon_t^T]$ allows us to account for fluctuations of the bound in Theorem 2 due to stochastic noise.

Corollary 2. *Let θ^* be a critical point for the loss $\mathcal{L}(\theta, \mathbf{x}, y)$ on \mathcal{D} . Let \mathbf{f}_{θ} denote a neural network with at least one hidden layer, with $\|\theta^1\| > 0$. Then,*

$$\frac{x_{\min}^2}{\|\theta^1\|_2^2} \mathbb{E}_{\mathcal{D}} \|\nabla_{\mathbf{x}} \mathcal{L}\|_2^2 \leq \text{tr}(S) + o(\mathcal{L}(\theta)) \quad (9)$$

with $S = C + \frac{1}{B} \mathbb{E}_{\mathcal{D}} [\nabla_{\theta} \mathcal{L}(\theta)] \mathbb{E}_{\mathcal{D}} [\nabla_{\theta} \mathcal{L}(\theta)]^T$ denoting the gradient uncentered covariance.

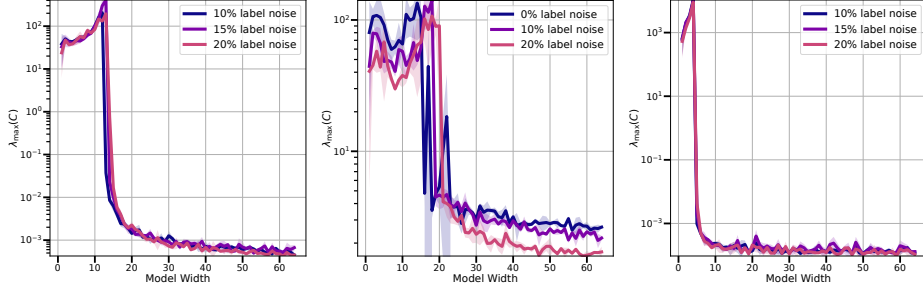


Figure 3: **Dominant noise-covariance eigenvalue.** (Top) From left to right: ConvNets trained on CIFAR-10 (left), CIFAR-100 (middle) and ResNets trained on CIFAR-10 (right). In all settings, the magnitude of stochastic noise strongly correlates with double descent, peaking at the interpolation threshold, and highlighting a nonlinear dependence on network width. All values are reported in log- y scale to better separate models in the interpolating regime.

Figure 3 shows the largest principal component of the gradient noise covariance C , as model size increases. Similarly to the mean curvature, stochastic noise strongly correlates with the Lipschitz constant, decreasing considerably in the interpolation regime, thus presenting an additional fundamental quantity strongly correlating with double descent.

Lastly, we conclude by discussing stability of Theorem 2 with respect to training hyperparameters.

Stability of the bound The dependency of Theorem 2 on SGD hyperparameters can be studied via the approximation error $\mathcal{L}(\theta) - \mathcal{L}(\theta^*)$ (Liu et al., 2021; Thomas et al., 2020).

Corollary 3. *Let θ^* be a critical point for the loss $\mathcal{L}(\theta, \mathbf{x}, y)$ on \mathcal{D} . Let \mathbf{f}_θ denote a neural network with at least one hidden layer, with $\|\theta^1\| > 0$. Then,*

$$\begin{aligned} \frac{x_{\min}^2}{\|\theta^1\|_2^2} \mathbb{E}_{\mathcal{D}} \|\nabla_{\mathbf{x}} \mathcal{L}\|_2^2 &\leq o(\mathcal{L}(\theta)) \quad + \\ \frac{\eta}{2(1-\mu)} \lambda_{\max} \left[\left(I_p - \frac{\eta}{2(1+\mu)} H \right)^{-1} C \right] \text{tr}(H) \end{aligned} \quad (10)$$

Specifically, the bound implies a well-known stability condition of θ^* : $\eta < \frac{4(\mu+1)}{\lambda_{\max}(H)}$ (Liu et al., 2021; Thomas et al., 2020).

Summary Our study of the Lipschitz constant reveals non-monotonic trends that strongly correlate with double descent for the test error, a phenomenon not captured by uniform bounds. By connecting the empirical Lipschitz to fundamental properties of the loss landscape, we present several correlates of double descent in parameter space, which in proximity of a critical point θ^* control complexity of the model function \mathbf{f}_θ on the training data \mathcal{D} .

Figure 4 summarizes our main findings, showing a strong correlation between the empirical Lipschitz constant and maximum parameter-space curvature of the loss landscape, mean parameter-space curvature, as well as the first principal component of gradient noise, with networks with large Lipschitz constant incurring in high test error.

Importantly, our analysis shows that for networks at convergence, the gradients $\nabla_{\theta} \mathcal{L}$ are bounded by the Hessian trace. Crucially, this implies that for large models, the loss $\mathcal{L}(\theta, \mathbf{x}, y)$ is Lipschitz also in θ . Essentially, our Theorem 2 is a special case of the Poincaré inequality, bounding a function through its gradient, which we apply to $\nabla_{\theta} \mathbf{f}$ via the chain rule. Intuitively, an analogous bound could be expected to hold for other families of compositional models.

Our analysis and experiments open many exciting questions on extending our observations beyond (i) piece-wise linear model functions, (ii) networks at convergence, as well as (iii) estimation of the Lipschitz on the training data. In section 4 we empirically explore these questions.

4 Implications for Implicit Regularization

We conclude our study by exploring broader implications of the trends observed in section 3. Section 4.1 extends our main finding to transformer architectures trained on machine translation tasks. Section 4.2 studies the development

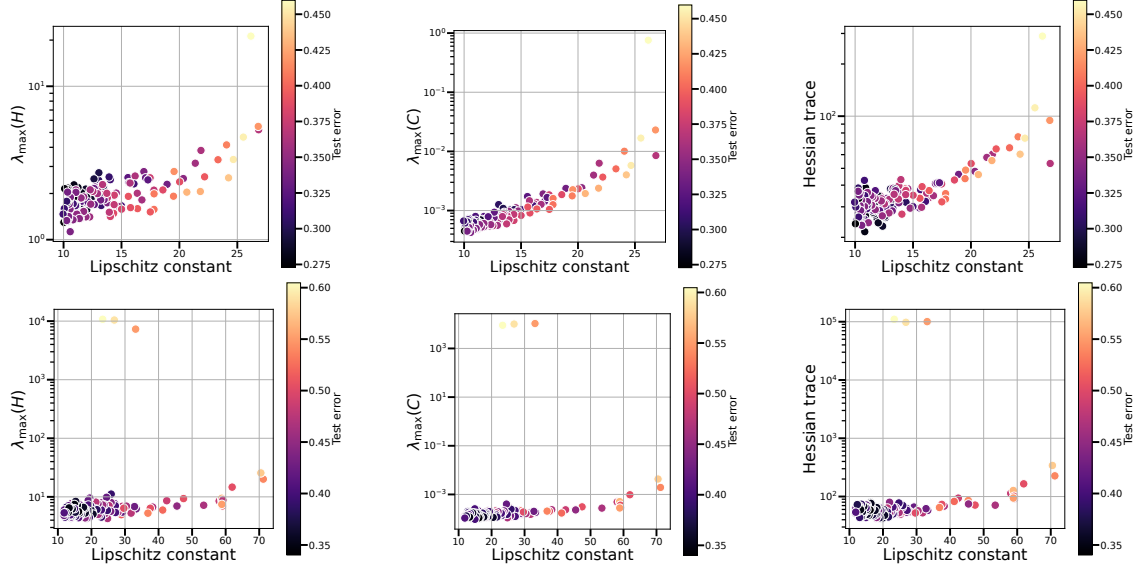


Figure 4: **Correlation between Lipschitz constant and parameter-space curvature.** From left to right: maximum curvature (left), dominant noise-covariance eigenvalue (middle) and mean curvature (right), respectively for ConvNets trained on CIFAR-10 (top), and ResNets trained on CIFAR-10 (bottom). In all settings, mean and maximum parameter-space curvature strongly correlate with the empirical Lipschitz constant in the interpolating regime. Furthermore, models with higher empirical Lipschitz present higher mean and maximum curvatures, and incur in higher test error. All values are reported in log- y scale to better separate models.

of the Lipschitz constant throughout epochs, while section 4.3 studies implications of our findings for understanding effective complexity of trained networks. Finally, section 4.4 extends our experimental findings beyond training data.

4.1 Beyond Piece-wise Linear Networks

We consider transformer architectures (Vaswani et al., 2017), whose model functions are not endowed with piece-wise linear geometry due to softmax-based attention. Following (Nakkiran et al., 2019), we train 8-layer multi-head attention transformers (Vaswani et al., 2017) on machine translation tasks, and control model size by scaling the embedding dimension h , as well as the width of hidden fully connected layers to $4h$. We compute Equation 2 on $\nabla_{\mathbf{x}}\mathcal{L}$, where \mathcal{L} is the per-token perplexity. We note that Equation 2 can still be applied to the Jacobian $\nabla_{\mathbf{x}}\mathcal{L}$ – which linearly approximates \mathcal{L} at each point \mathbf{x} – and the expected operator norm should be intended as the Sobolev seminorm $\|\mathcal{L}\|_{\mathcal{D},1,2}$ of \mathcal{L} on \mathcal{D} . Figure 5 extends our main finding, showing that the Sobolev seminorm of \mathcal{L} depends non-monotonically on model size, peaking near the interpolation threshold, and extending our main result beyond vision architectures.

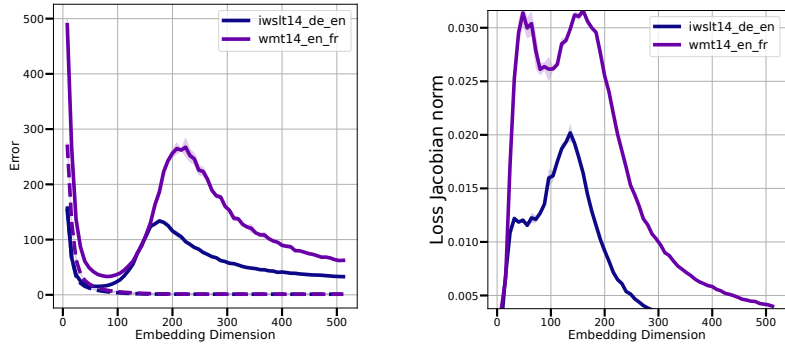


Figure 5: (Left) **Double descent** of the test error for transformers trained on translation tasks, as the embedding dimension and model width vary. (Right) **Loss Sobolev norm**.

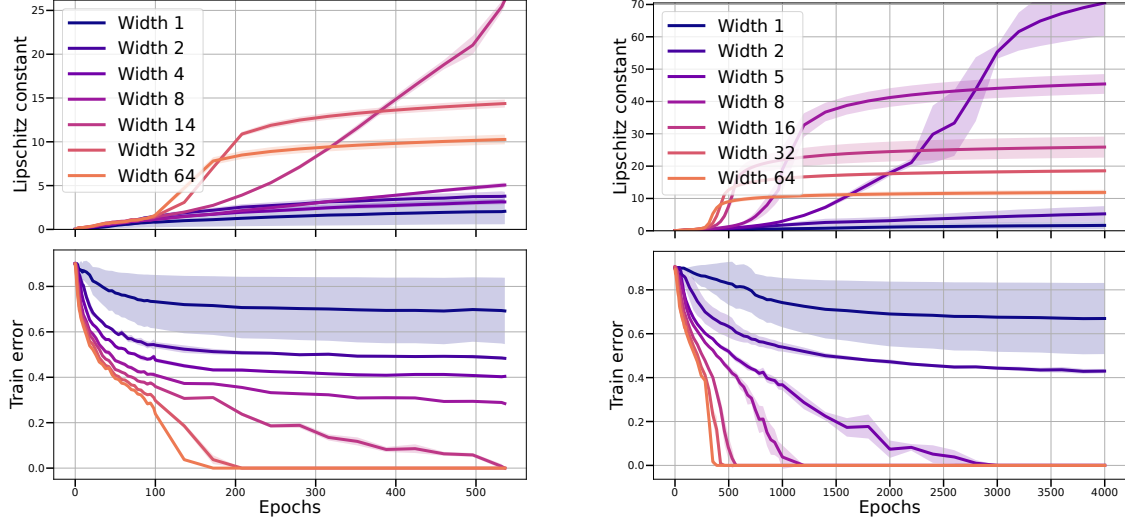


Figure 6: (Top) **Lipschitz constant over epochs** and (Bottom) **Train error**, for ConvNets (left) and ResNets (right) trained on CIFAR-10 with 20% noisy labels.

4.2 Overparameterization Accelerates Interpolation

Our experimental setup so far only focused on networks at convergence. Here, we track the development of the empirical Lipschitz throughout training, in relationship to the training error (0/1 loss), providing deeper insights on effective model complexity. Figure 6 (top) shows the Lipschitz constant of ConvNets (left) and ResNet18s (right) trained on CIFAR-10 with 20% noisy training labels, for representative model widths, together with the respective training error (bottom). Heatmaps for all model widths are presented in appendix C.2, connecting to the test error in Figure 10. We recall that the model-wise interpolation threshold (Belkin et al., 2019) denotes the smallest model width ω_0 that perfectly classifies the training set, in our experiment corresponding to $\omega_0 = 14$ for ConvNets, and $\omega_0 = 5$ for ResNets. We train ConvNets for 500 epochs, and ResNets for 4k epochs, to ensure a fair training budget. During training, we observe three distinct behaviours.

Small models ($\omega \ll \omega_0$) are unable to interpolate the entire training set, and their training error as well as empirical Lipschitz quickly plateau, remaining stable therefrom. Increasing size among small models reduces their training error, and correspondingly increases the Lipschitz.

At the same time, models near the interpolation threshold ω_0 – peaking in test error and Lipschitz (cfr. Figure 1) – are able to achieve interpolation, *only when given considerable training budget*. Correspondingly, the Lipschitz monotonically increases over training as the training error is reduced, resulting in models achieving worst Lipschitz and worst test error. In contrast, consistently with the double descent trends reported in section 3, large models ($\omega \gg \omega_0$) are able to quickly interpolate the training set, with the largest models requiring fewer epochs to achieve interpolation.

Implications The seemingly unbounded Lipschitz constant of models near the threshold ω_0 suggests that the observations reported in Hardt et al. (2016) – for which prolonged training budgets may hurt generalization performance – are pertaining only to models near the threshold. In fact, larger models can be trained for considerably long without a comparable increase in complexity. Furthermore, the notion of acceleration via overparameterization was formally studied by Arora et al. (2018), showing that convergence of linear networks is accelerated by overparameterization via increasing network depth, *irrespective of model width*. In contrast, our findings show that for non-linear networks, model width considerably affects the speed of convergence.

4.3 Overparameterization Constrains Complexity

Referring again to Figure 6, we now consider implications for effective complexity of trained networks. First, since model weights are typically initialized to small values around zero (He et al., 2015; Glorot & Bengio, 2010), the Lipschitz constant of all models is close to zero at the beginning of training. This corresponds to each model expressing a very simple function (low empirical Lipschitz), albeit with low generalization performance (typically close to random chance). Second, during training, fitting the dataset requires all models’ Lipschitz constant to

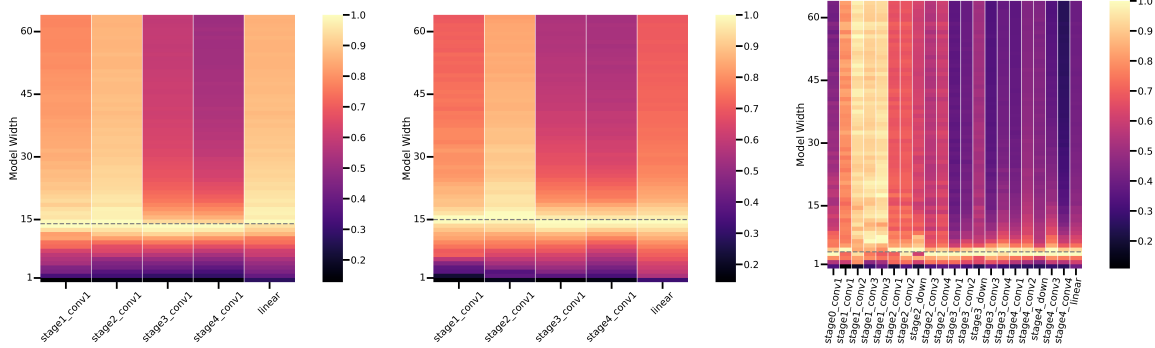


Figure 7: **Distance from initialization for each layer** of ConvNets trained on CIFAR-10 with 20% noisy labels (left), CIFAR-100 (middle), and ResNet18s trained on CIFAR-10 with 20% noisy labels (right). For each ConvNet and most ResNet layers, distance of the converged layer’s parameters from initialization follows double descent, peaking at the interpolation threshold (dashed), suggesting global boundedness of the model function beyond training data for large models.

grow, with corresponding increase in model complexity (as measured by Equation 3). When zero error is reached ($\omega \geq \omega_0$), the Lipschitz constant approximately plateaus, thereafter only slowly increasing over epochs. Recalling that large models are observed to interpolate faster, this finding suggest that large models may achieve interpolation via least meaningful deviation from initialization, realizing an overall smooth function.

To assess our hypothesis, we study distance from initialization $\|\theta_T^\ell - \theta_0^\ell\|_F$ of each layer ℓ , with θ_0^ℓ and θ_T^ℓ respectively denoting the layers’ weights at initialization and convergence. Figure 7 presents distance from initialization (colour) as model width increases (y -axis), for each layer (x -axis), for ConvNets (left) and ResNets (right) trained on CIFAR-10 with 20% label noise, and ConvNets on CIFAR-100 with no label noise (middle). For each heatmap independently, the distance from initialization of each layer is normalized by the largest distance observed for that layer.

Intriguingly, for almost all layers, the quantity follows double descent as model width increases, peaking near the interpolation threshold, and matching the epoch-wise trend reported in section 4.2. Importantly, the largest distance from initialization is observed for the later layers, counting the largest number of parameters, whose role has been recently connected to memorization (Stephenson et al., 2021).

Implications This exciting finding supports our interpretation that faster interpolation, as promoted by overparameterization, results in model functions which are overall low-complexity, due to least (but meaningful) deviation from initialization. Our proposed interpretation corroborates the empirical observations of Gamba et al. (2022a) and Somepalli et al. (2022), who respectively report that large models express low curvature model functions in input space, and consistent decision boundaries. Finally, our findings extend Neyshabur et al. (2018), who initially reported that distance from initialization decreases for overparameterized models. Importantly, we show that the statistic is non-monotonic in model size, and that it strongly correlates with double descent for the test error, and the overall trends observed in this work. Together with the observed low curvature of large models shown in section 3.4, this finding shares potential connection to the linear mode connectivity phenomenon (Garipov et al., 2018), by which low-loss paths that connect solutions obtained by optimization of the same model and task have been found in practice.

4.4 Bounded Complexity Beyond Training Data

To conclude, in Figure 8 we estimate the empirical Lipschitz of ConvNets (left) and ResNets (right) trained on CIFAR%-10, probing the networks by computing Equation 2 on unseen test data or with random noise (experimental details in appendix E). We report that, surprisingly, even for data lying far from the support of the data distribution, the empirical Lipschitz constant remains bounded, and the model-wise trend follows double descent, peaking at the interpolation threshold. This finding further strengthens the view that reduced distance from initialization via acceleration may essentially control complexity of the *whole* model function. This suggests it may be possible to cast implicit regularization as reduced distance from initialization (akin to weight decay). We leave this exciting direction to future work.

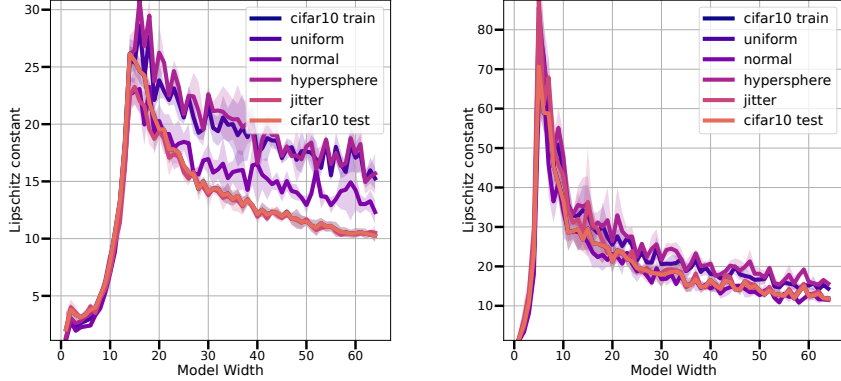


Figure 8: **Lipschitz constant estimated on random validation data** for ConvNets (left) and ResNets (right) trained on CIFAR-10 with 20% noisy labels. Confirming our interpretation, even far from the support of the data distribution, the models’ Lipschitz follows double descent, supporting the notion of globally bounded model function due to reduced distance from initialization for overparameterized models.

5 Related Work and Discussion

While deep neural networks are able to express a rich family of functions as their model size increases (Zhang et al., 2018; Telgarsky, 2016; Cybenko, 1989), the effective complexity of generalizing models appears to be constrained in practice (Neyshabur et al., 2018; Zhang et al., 2019; Neyshabur et al., 2015b). Developing a formal characterization of the mechanisms driving such phenomenon is still a challenging open problem. Theoretical studies hinge upon finding a parameterization of the hypothesis class of trained networks that meaningfully constrains their expressivity. Importantly, several works rely on uniform upper bounds on the Lipschitz to constrain model function variation (Kawaguchi et al., 2022; Ma & Ying, 2021; Wei & Ma, 2019; Nagarajan & Kolter, 2018; Bartlett et al., 2017). Furthermore, in practical settings, achieving low Lipschitz has been connected to improved generalization performance (Gouk et al., 2021; Moosavi-Dezfooli et al., 2019; Novak et al., 2018).

Recently, the study of the Lipschitz constant has received renewed attention, with Bubeck & Sellke (2021) prescribing overparameterization as a necessary condition for smooth interpolation of training data, for a generic class of learners. Our work corroborates their findings, by also presenting an upper bound on the Lipschitz in terms of neural networks fundamental components, in relation to optimization and the loss landscape in parameter space. Our results highlight the importance of incorporating the optimizer into the hypothesis class of neural networks.

While tightly estimating the Lipschitz constant is NP-hard for deep networks (Jordan & Dimakis, 2020; Virmaux & Scaman, 2018), we focus on the function applied by ReLU networks on the training data, and present relative trends as model size increases. Crucially, we extend a uniform bound on empirical Lipschitz Ma & Ying (2021), by proposing a novel one that experimentally captures double descent, in light of recently proposed models of stochastic noise in proximity of minima of the loss (Ziyin et al., 2022; Mori et al., 2022; Li et al., 2021; Thomas et al., 2020).

Interestingly a concurrent work uses Sobolev seminorms of ReLU networks on the training set to propose a model complexity measure Dherin et al. (2022). In line with our findings, their proposed measure captures the test error. Our works differ in that they focus on studying explicit and implicit regularization of the metric, while instead we build a theoretical connection to several fundamental quantities capturing double descent in connection to the geometry of the loss landscape. Importantly, we extend our findings beyond training data, with evidence of global boundedness of the model function through distance from initialization, which we are the first to study in relation to double descent.

Limitations The analysis presented in section 3.4 holds only in proximity of a critical point, and does not account for the high-dimensional trajectories taken by SGD in parameter space far from a solution θ^* , nor for how such solution is found in the loss landscape. Furthermore, the stability analysis presented in corollaries 2 and 3 accounts only for covariance of stochastic noise ϵ_t with respect to mini-batch sampling ξ_t , and does not account for dependence on θ_t , which is controlled by a power law (Mori et al., 2022). In this work, we focus on empirically establishing a non-monotonic dependency of C and H from model size, highlighting a strong correlation with the Lipschitz constant, as well as double descent for the test error in practical settings. A more precise analysis of our

bounds would require accounting for the parameters covariance $\mathbb{E}_{\theta}[\theta_t \theta_t^T]$ at each iteration t , which we leave for future work.

6 Conclusions

We present an extensive study of the empirical Lipschitz of deep networks undergoing double descent, questioning the informativeness of uniform upper bounds on the constant, which may hide effective model complexity. By building a theoretical connection with the geometry of the loss landscape, we present several correlates of double descent in terms of fundamental notions, which we hope will inspire further theoretical studies. Our work isolates two important quantities – namely loss landscape flatness and distance of parameters from initialization – respectively controlling optimization dynamics around a critical point and bounding model function complexity beyond the training data. We believe understanding the structure and singularity of the overparameterized mapping from parameters to model functions is a fundamental open problem, which might reveal a causal structure between the correlates of double descent reported in this work.

References

Sanjeev Arora, Nadav Cohen, and Elad Hazan. On the optimization of deep networks: Implicit acceleration by overparameterization. In *Proceedings of the 35th International Conference on Machine Learning*, volume 80 of *Proceedings of Machine Learning Research*, pp. 244–253. PMLR, 10–15 Jul 2018.

Devansh Arpit, Víctor Campos, and Yoshua Bengio. How to initialize your network? robust initialization for weightnorm & resnets. *Advances in Neural Information Processing Systems*, 32, 2019.

Peter L Bartlett, Dylan J Foster, and Matus J Telgarsky. Spectrally-normalized margin bounds for neural networks. *Advances in neural information processing systems*, 30, 2017.

Peter L. Bartlett, Philip M. Long, Gábor Lugosi, and Alexander Tsigler. Benign overfitting in linear regression. *Proceedings of the National Academy of Sciences*, 117(48):30063–30070, 2020. doi: 10.1073/pnas.1907378117.

Mikhail Belkin, Daniel J Hsu, and Partha Mitra. Overfitting or perfect fitting? risk bounds for classification and regression rules that interpolate. In S. Bengio, H. Wallach, H. Larochelle, K. Grauman, N. Cesa-Bianchi, and R. Garnett (eds.), *Advances in Neural Information Processing Systems*, volume 31. Curran Associates, Inc., 2018.

Mikhail Belkin, Daniel Hsu, Siyuan Ma, and Soumik Mandal. Reconciling modern machine-learning practice and the classical bias–variance trade-off. *Proceedings of the National Academy of Sciences*, 116(32):15849–15854, 2019.

Glenn W Brier. Verification of forecasts expressed in terms of probability. *Monthly Weather Review*, 78(1):1–3, 1950.

Sébastien Bubeck and Mark Sellke. A universal law of robustness via isoperimetry. *Advances in Neural Information Processing Systems*, 34, 2021.

Mauro Cettolo, Christian Girardi, and Marcello Federico. Wit3: Web inventory of transcribed and translated talks. In *Proceedings of the Conference of European Association for Machine Translation (EAMT)*, pp. 261–268, 2012.

George Cybenko. Approximation by superpositions of a sigmoidal function. *Mathematics of control, signals and systems*, 2(4):303–314, 1989.

Alexandre De Brébisson and Pascal Vincent. An exploration of softmax alternatives belonging to the spherical loss family. *International Conference on Learning Representations*, 2016.

Benoit Dherin, Michael Munn, Mihaela Rosca, and David GT Barrett. Why neural networks find simple solutions: the many regularizers of geometric complexity. *arXiv preprint arXiv:2209.13083*, 2022.

Matteo Gamba, Adrian Chmielewski-Anders, Josephine Sullivan, Hossein Azizpour, and Mårten Björkman. Are all linear regions created equal? In *International Conference on Artificial Intelligence and Statistics*, pp. 6573–6590. PMLR, 2022a.

Matteo Gamba, Erik Englesson, Mårten Björkman, and Hossein Azizpour. Deep double descent via smooth interpolation. *arXiv preprint arXiv:2209.10080*, 2022b.

Timur Garipov, Pavel Izmailov, Dmitrii Podoprikhin, Dmitry P Vetrov, and Andrew G Wilson. Loss surfaces, mode connectivity, and fast ensembling of dnns. In S. Bengio, H. Wallach, H. Larochelle, K. Grauman, N. Cesa-Bianchi, and R. Garnett (eds.), *Advances in Neural Information Processing Systems*. Curran Associates, Inc., 2018.

Mario Geiger, Stefano Spigler, Stéphane d’Ascoli, Levent Sagun, Marco Baity-Jesi, Giulio Biroli, and Matthieu Wyart. Jamming transition as a paradigm to understand the loss landscape of deep neural networks. *Physical Review E*, 100(1):012115, 2019.

Xavier Glorot and Yoshua Bengio. Understanding the difficulty of training deep feedforward neural networks. In *Proceedings of the thirteenth international conference on artificial intelligence and statistics*, pp. 249–256. JMLR Workshop and Conference Proceedings, 2010.

Henry Gouk, Eibe Frank, Bernhard Pfahringer, and Michael J Cree. Regularisation of neural networks by enforcing lipschitz continuity. *Machine Learning*, 110(2):393–416, 2021.

Boris Hanin and David Rolnick. Complexity of linear regions in deep networks. In *International Conference on Machine Learning*, pp. 2596–2604, 2019a.

Boris Hanin and David Rolnick. Deep relu networks have surprisingly few activation patterns. In *Advances in Neural Information Processing Systems*, pp. 359–368, 2019b.

Moritz Hardt, Ben Recht, and Yoram Singer. Train faster, generalize better: Stability of stochastic gradient descent. In Maria Florina Balcan and Kilian Q. Weinberger (eds.), *Proceedings of The 33rd International Conference on Machine Learning*, volume 48 of *Proceedings of Machine Learning Research*, pp. 1225–1234, New York, New York, USA, 20–22 Jun 2016. PMLR.

Kaiming He, Xiangyu Zhang, Shaoqing Ren, and Jian Sun. Delving deep into rectifiers: Surpassing human-level performance on imagenet classification. In *Proceedings of the IEEE International Conference on Computer Vision*, pp. 1026–1034, 2015.

Yohei Hosoe and Tomomichi Hagiwara. On second-moment stability of discrete-time linear systems with general stochastic dynamics. *IEEE Transactions on Automatic Control*, 67(2):795–809, 2022. doi: 10.1109/TAC.2021.3057994.

Michael F Hutchinson. A stochastic estimator of the trace of the influence matrix for laplacian smoothing splines. *Communications in Statistics-Simulation and Computation*, 19(2):433–450, 1990.

Matt Jordan and Alexandros G Dimakis. Exactly computing the local lipschitz constant of relu networks. In H. Larochelle, M. Ranzato, R. Hadsell, M.F. Balcan, and H. Lin (eds.), *Advances in Neural Information Processing Systems*, volume 33, pp. 7344–7353. Curran Associates, Inc., 2020.

Kenji Kawaguchi, Zhun Deng, Kyle Luh, and Jiaoyang Huang. Robustness implies generalization via data-dependent generalization bounds. In Kamalika Chaudhuri, Stefanie Jegelka, Le Song, Csaba Szepesvari, Gang Niu, and Sivan Sabato (eds.), *Proceedings of the 39th International Conference on Machine Learning*, volume 162 of *Proceedings of Machine Learning Research*, pp. 10866–10894. PMLR, 17–23 Jul 2022.

Alex Krizhevsky, Geoffrey Hinton, et al. Learning multiple layers of features from tiny images. Master’s thesis, University of Toronto, 2009.

Daniel LeJeune, Randall Balestrieri, Hamid Javadi, and Richard G Baraniuk. Implicit rugosity regularization via data augmentation. *arXiv preprint arXiv:1905.11639*, 2019.

Zhiyuan Li, Tianhao Wang, and Sanjeev Arora. What happens after sgd reaches zero loss?—a mathematical framework. In *International Conference on Learning Representations*, 2021.

Kangqiao Liu, Liu Ziyin, and Masahito Ueda. Noise and fluctuation of finite learning rate stochastic gradient descent. In Marina Meila and Tong Zhang (eds.), *Proceedings of the 38th International Conference on Machine Learning*, volume 139 of *Proceedings of Machine Learning Research*, pp. 7045–7056. PMLR, 18–24 Jul 2021.

Chao Ma and Lexing Ying. On linear stability of sgd and input-smoothness of neural networks. *Advances in Neural Information Processing Systems*, 34:16805–16817, 2021.

Matouš Macháček and Ondřej Bojar. Results of the wmt14 metrics shared task. In *Proceedings of the Ninth Workshop on Statistical Machine Translation*, pp. 293–301, 2014.

Harsh Mehta, Ashok Cutkosky, and Behnam Neyshabur. Extreme memorization via scale of initialization. In *International Conference on Learning Representations*, 2020.

Guido F Montufar, Razvan Pascanu, Kyunghyun Cho, and Yoshua Bengio. On the number of linear regions of deep neural networks. In *Advances in Neural Information Processing Systems*, pp. 2924–2932, 2014.

Seyed-Mohsen Moosavi-Dezfooli, Alhussein Fawzi, Jonathan Uesato, and Pascal Frossard. Robustness via curvature regularization, and vice versa. In *Proceedings of the IEEE/CVF Conference on Computer Vision and Pattern Recognition (CVPR)*, June 2019.

Takashi Mori, Liu Ziyin, Kangqiao Liu, and Masahito Ueda. Power-law escape rate of SGD. In Kamalika Chaudhuri, Stefanie Jegelka, Le Song, Csaba Szepesvari, Gang Niu, and Sivan Sabato (eds.), *Proceedings of the 39th International Conference on Machine Learning*, volume 162 of *Proceedings of Machine Learning Research*, pp. 15959–15975. PMLR, 17–23 Jul 2022.

Vaishnavh Nagarajan and Zico Kolter. Deterministic pac-bayesian generalization bounds for deep networks via generalizing noise-resilience. In *International Conference on Learning Representations*, 2018.

Preetum Nakkiran, Gal Kaplun, Yamini Bansal, Tristan Yang, Boaz Barak, and Ilya Sutskever. Deep double descent: Where bigger models and more data hurt. In *International Conference on Learning Representations*, 2019.

Behnam Neyshabur, Ryota Tomioka, and Nathan Srebro. Norm-based capacity control in neural networks. In *Conference on Learning Theory*, pp. 1376–1401. PMLR, 2015a.

Behnam Neyshabur, Ryota Tomioka, and Nathan Srebro. In search of the real inductive bias: On the role of implicit regularization in deep learning. In *International Conference on Learning Representations Workshop Track*, 2015b.

Behnam Neyshabur, Zhiyuan Li, Srinadh Bhojanapalli, Yann LeCun, and Nathan Srebro. The role of over-parametrization in generalization of neural networks. In *International Conference on Learning Representations*, 2018.

Roman Novak, Yasaman Bahri, Daniel A Abolafia, Jeffrey Pennington, and Jascha Sohl-Dickstein. Sensitivity and generalization in neural networks: an empirical study. In *International Conference on Learning Representations*, 2018.

Barak A Pearlmutter. Fast exact multiplication by the hessian. *Neural computation*, 6(1):147–160, 1994.

Maithra Raghu, Ben Poole, Jon Kleinberg, Surya Ganguli, and Jascha Sohl-Dickstein. On the expressive power of deep neural networks. In *International Conference on Machine Learning*, pp. 2847–2854, 2017.

Kevin Roth, Yannic Kilcher, and Thomas Hofmann. Adversarial training is a form of data-dependent operator norm regularization. *Advances in Neural Information Processing Systems*, 33:14973–14985, 2020.

Gowthami Somepalli, Liam Fowl, Arpit Bansal, Ping Yeh-Chiang, Yehuda Dar, Richard Baraniuk, Micah Goldblum, and Tom Goldstein. Can neural nets learn the same model twice? investigating reproducibility and double descent from the decision boundary perspective. In *Proceedings of the IEEE/CVF Conference on Computer Vision and Pattern Recognition*, pp. 13699–13708, 2022.

Cory Stephenson, suchismita padhy, Abhinav Ganesh, Yue Hui, Hanlin Tang, and SueYeon Chung. On the geometry of generalization and memorization in deep neural networks. In *International Conference on Learning Representations*, 2021.

Matus Telgarsky. Benefits of depth in neural networks. In *29th Annual Conference on Learning Theory*, volume 49 of *Proceedings of Machine Learning Research*, pp. 1517–1539, Columbia University, New York, New York, USA, 23–26 Jun 2016. PMLR.

Valentin Thomas, Fabian Pedregosa, Bart van Merriënboer, Pierre-Antoine Manzagol, Yoshua Bengio, and Nicolas Le Roux. On the interplay between noise and curvature and its effect on optimization and generalization. In Silvia Chiappa and Roberto Calandra (eds.), *Proceedings of the Twenty Third International Conference on Artificial Intelligence and Statistics*, volume 108 of *Proceedings of Machine Learning Research*, pp. 3503–3513. PMLR, 26–28 Aug 2020.

Ashish Vaswani, Noam Shazeer, Niki Parmar, Jakob Uszkoreit, Llion Jones, Aidan N Gomez, Łukasz Kaiser, and Illia Polosukhin. Attention is all you need. *Advances in neural information processing systems*, 30, 2017.

Aladin Virmaux and Kevin Scaman. Lipschitz regularity of deep neural networks: analysis and efficient estimation. *Advances in Neural Information Processing Systems*, 31, 2018.

Colin Wei and Tengyu Ma. Data-dependent sample complexity of deep neural networks via lipschitz augmentation. *Advances in Neural Information Processing Systems*, 32, 2019.

Lei Wu and Chao Ma. How sgd selects the global minima in over-parameterized learning: A dynamical stability perspective. *Advances in Neural Information Processing Systems*, 31, 2018.

Chiyuan Zhang, Samy Bengio, Moritz Hardt, Benjamin Recht, and Oriol Vinyals. Understanding deep learning requires rethinking generalization. *International Conference on Learning Representations*, 2018.

Chiyuan Zhang, Samy Bengio, and Yoram Singer. Are all layers created equal? *ICML Workshop Deep Phenomena*, 2019.

Liu Ziyin, Kangqiao Liu, Takashi Mori, and Masahito Ueda. Strength of minibatch noise in SGD. In *International Conference on Learning Representations*, 2022.

A Appendix

Section B fully details our experimental setup. Section C presents additional experiments, empirically showing that the non-monotonic trends reported for the loss gradients in the main paper are caused by the model function f underlying the loss. Section D details the algorithms used for estimating the empirical Lipschitz constant and to collect statistics about parameter space curvature. Then, section E describes the distributions used for generating random validation data for the experiment in section 4.4. Finally, section F presents proofs of the formal statements of section 3.

B Experimental Setup

Following Nakkiran et al. (2019), we train a family of ConvNets composed of 4 convolutional stages – each corresponding to a [Conv, ReLU] block followed by maxpooling with stride 2 – and 1 dense classification layer. We also train a family of ResNet18s (He et al., 2015) without batch normalization layers. Both network architectures are composed of 4 convolutional stages, in which each spatial dimension is reduced by factor of 2 and the number of learned feature maps doubles. More precisely, the convolutional stages respectively follow the progression $[\omega, 2\omega, 4\omega, 8\omega]$, where ω is the base width of the network, i.e. the number of feature maps learned at the first layer.

In our experiments, we vary the base width in the range $\omega = 1, \dots, 64$. By controlling the network size through the network width, we produce a range of models presenting model-wise double descent in the test error, which captures the essence of the *benign overfitting* phenomenon (Bartlett et al., 2020) observed for large interpolating networks, while also presenting *malign overfitting* for models near the interpolation threshold. Furthermore, controlling model size through base width allows us to keep the network depth fixed, and focus our study on effective complexity of fixed-depth networks, for two network architecture families (ConvNets and ResNets).

To tune hyperparameters, we take a random validation split of size 1000 from each CIFAR training set. We train all networks with SGD with momentum 0.9, batch size 128, and fixed learning rate, set at $\eta = 5e-3$ for the ConvNets and $\eta = 1e-4$ for the ResNets. We train the ConvNets for 500 epochs, and the ResNets for 4000. To stabilize prolonged training, we use learning rate warmup over the first 5 epochs of training, starting from a learning rate $\eta_0 = 10^{-1} \times \eta$.

Transformer Architectures We also consider multi-head attention-based Transformers (Vaswani et al., 2017) for neural machine translation tasks. We vary model size by controlling the embedding dimension d_e , as well as the width h of all fully connected layers, which we set to $h = 4d_e$ following the architecture described in Vaswani et al. (2017). We train the transformer networks on the WMT’14 En-Fr task (Macháček & Bojar, 2014), as well as ISWLT’14 De-En (Cettolo et al., 2012). The training set of WMT’14 is reduced by randomly sampling 200k sentences, fixed for all models. The networks are trained for 80k gradient steps, to optimize per-token perplexity, with 10% label smoothing, and no dropout, gradient clipping or weight decay.

Hardware specifications Our codebase is implemented in Pytorch version 1.11, running on a local cluster equipped with NVIDIA A100 GPUs with 40GB onboard memory. Our experiments involve training 64 ConvNets and ResNets (each corresponding to a base width ω) for up to 4000 epochs, producing 72 model checkpoints per network. We use 3 random seeds for the ConvNets and 5 for the ResNets, controlling network initialization and the shuffling and sampling of mini-batches from the training set. We use a dedicated random seed for generating the validation split used for hyperparameter tuning, fixed for all networks, as well as a fixed seed for corrupting the CIFAR training labels. The Lipschitz constant is estimated and averaged on every training point for each of the reported configurations.

Number of model parameters Our main empirical finding is that, while network size increases – causing uniform upper bounds like Ma & Ying (2021) (Theorem 3) to monotonically increase – the empirical Lipschitz constant of the models decreases past the interpolation threshold. To better frame our observations, we report in Table 1 the number of parameters for a few representative models in our experiments.

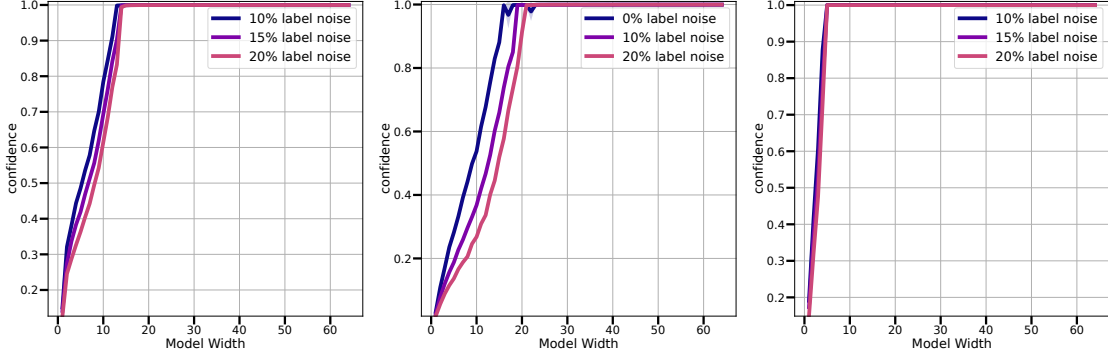


Figure 9: **Prediction confidence** as a function of model size, for ConvNets trained on CIFAR-10 (left), CIFAR-100 (middle) and ResNet18s trained on CIFAR-10. For all experimental settings, the model confidence monotonically depends on model size. By Equation 16, this confirms that the non-monotonic trends reported in this work are caused by the model function f .

C Additional Experiments

C.1 Model Confidence

Our main theoretical results study the relationship between input-space gradients and parameter-space gradients of the loss \mathcal{L} . In this section, study the gradient decomposition of Equation 16, to isolate the dependency of the term $\mathbf{p}_n - \mathbf{e}_{y_n}$ from model size. Figure 9 shows that model confidence monotonically depends on model size. This highlights the fact that the double descent trends observed throughout this paper are to be attributed to the model function, as shown throughout our experiments for the empirical Lipschitz constant.

C.2 Empirical Lipschitz Throughout Training

In this section, we complement the results shown for selected model widths in Figure 6, by plotting the development of the empirical Lipschitz constant throughout training for all model sizes, and discuss its relationship to the test error. Extending our finding to additional model widths, Figure 10 shows that small models maintain a small Lipschitz constant throughout training, while models near the interpolation threshold accumulate a large Lipschitz after prolonged training. Finally, large models maintain a relatively low Lipschitz, plateauing earlier as model size increases past the interpolating threshold.

At the same time, with reference to the line plots in Figure 6, for all models the initial increase in Lipschitz constant – occurring during “early” training (up until epoch 100 for ConvNets and 400 for ResNets) – is matched by a rapid decrease in test error. During mid-training (epoch e $100 < e < 200$ for ConvNets, and $400 < e < 500$ for ResNets) the rate of increase of the Lipschitz constant changes according to model size. Small models plateau in their Lipschitz, train and test error, and remain stable thereafter. Models near the interpolation threshold start slowly increasing the Lipschitz constant as they slowly interpolate the training set, with corresponding increase in test error, showcasing the “malign overfitting” phenomenon (Bartlett et al., 2020). Strikingly, large models quickly interpolate the training set, causing relative increase in the Lipschitz constant, inversely correlating with model size.

Table 1: Number of model parameters p for representative widths ω on CIFAR-10. Models near the interpolation threshold are marked in bold.

ω	ConvNet	ResNet18
1	510	2,902
2	1,766	11,242
4	6,546	44,266
8	25,178	175,690
16	98,730	700,042
32	390,986	2,794,762
64	1,556,106	11,168,266

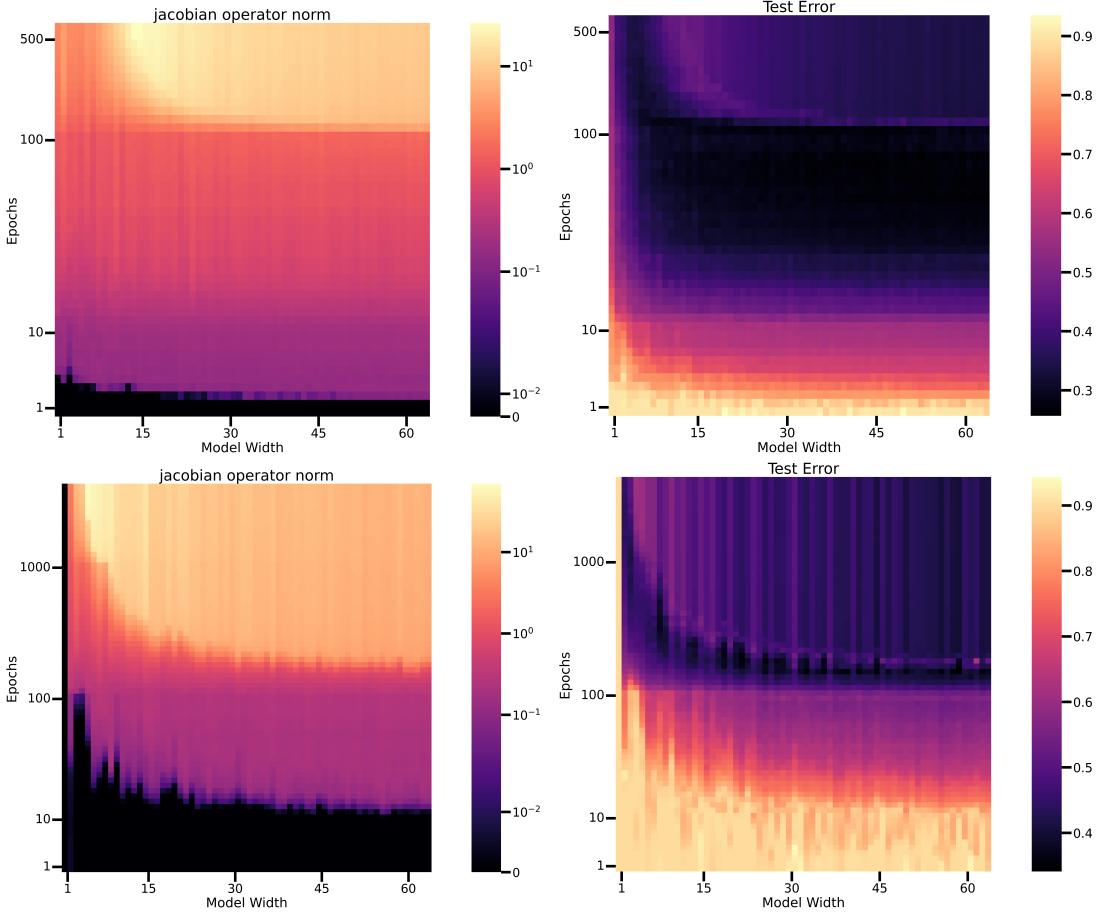


Figure 10: (Top left) **Empirical Lipschitz constant** (color) as a function of training epochs (y – axis) and model size (x -axis). (Top right) **Test error** for ConvNets trained on CIFAR-10 with 20% noisy training labels. (Bottom) Analogous plots for ResNet18s trained on the same dataset.

Throughout this phase of “accelerated interpolation” the test error undergoes epoch-wise double descent (Nakkiran et al., 2019). Crucially, while for all models the Lipschitz constant is monotonically increasing in epochs, the *rate* at which the Lipschitz grows correlates with *epoch-wise* double descent for the test error. This observation suggests that tracking second order information of \mathbf{f}_θ in input space may reveal important properties of interpolation. Indeed, input-space Hessian based measures (Moosavi-Dezfooli et al., 2019; LeJeune et al., 2019) have been observed to correlate with model performance for fixed-sized models. Our observations suggest that input-space curvature may bear significance for understanding epoch-wise double descent. We leave this exciting direction to future work.

D Operator Norm Estimation

For linear operators $\mathbf{A} : (\mathbb{R}^d, \|\cdot\|_p) \rightarrow (\mathbb{R}^K, \|\cdot\|_q)$, the operator norm is defined as

$$\|\mathbf{A}\|_{\text{op}} := \sup_{\mathbf{x}: \|\mathbf{x}\|_p \neq 0} \frac{\|\mathbf{A}\mathbf{x}\|_q}{\|\mathbf{x}\|_p}, \quad (11)$$

where the norms $\|\cdot\|_p$ and $\|\cdot\|_q$ are respectively taken in input and logit space. Crucially, if $p = q = 2$, then the operator norm can be estimated by computing the largest singular value of \mathbf{A} . For any data point $\bar{\mathbf{x}} \in \mathbb{R}^d$, evaluating the Jacobian at $\bar{\mathbf{x}}$ yields $\nabla_{\mathbf{x}} \mathbf{f}(\mathbf{x}, \theta)|_{\mathbf{x}=\bar{\mathbf{x}}} = \theta_\epsilon$, i.e. the linear function computed by \mathbf{f} on the activation region ϵ of $\bar{\mathbf{x}}$. Hence, at each point, $\|\mathbf{W}_\epsilon\|_{\text{op}}$, provides an estimate of worst-case sensitivity of the corresponding linear “piece” of \mathbf{f} . We note that, while the supremum $\|\mathbf{A}\|_{\text{op}}$ may not be attained within the activation region of $\bar{\mathbf{x}}$, the operator norm upper bounds worst-case sensitivity within the region. Furthermore, activation regions neighbouring training data tend to compute approximately the same linear function (Gamba et al., 2022a; Roth et al., 2020).

Computing the operator norm Computing the operator norm of $\theta_\epsilon \in \mathbb{R}^{K \times d}$ entails two steps. First, computing the gradient $\nabla_{\mathbf{x}} \mathbf{f}|_{\mathbf{x}=\bar{\mathbf{x}}} = \theta_\epsilon$ (via automatic differentiation), and then estimating its largest singular value. To perform the latter, we use a standard power method. Starting at iteration $t = 0$ with randomly initialized vectors $\tilde{\mathbf{u}}_0 \in \mathbb{R}^K$, $\tilde{\mathbf{v}}_0 \in \mathbb{R}^d$, and corresponding normalized vectors $\mathbf{u}_0 = \frac{\tilde{\mathbf{u}}_0}{\|\tilde{\mathbf{u}}_0\|_q}$, $\mathbf{v}_0 = \frac{\tilde{\mathbf{v}}_0}{\|\tilde{\mathbf{v}}_0\|_p}$, at step t we compute

$$\begin{aligned}\tilde{\mathbf{u}}_t &\leftarrow \nabla_{\mathbf{x}} \mathbf{f} \mathbf{v}_{t-1} \\ \tilde{\mathbf{v}}_t &\leftarrow \mathbf{u}_t^T \nabla_{\mathbf{x}} \mathbf{f} \\ \sigma_t &\leftarrow \mathbf{u}_t^T \nabla_{\mathbf{x}} \mathbf{f} \mathbf{v}_t\end{aligned}\tag{12}$$

with σ_t storing the largest singular value at convergence, defined based on a relative tolerance $1e - 6$ on the size of the increments of σ_t .

In our experiments, we estimate the Lipschitz constant of the network by its empirical constant, $\gamma_N = \frac{1}{N} \sum_{n=1}^N \|\nabla_{\mathbf{x}} \mathbf{f}|_{\mathbf{x}=\mathbf{x}_n}\|_{\text{op}}$, for all training points $\mathbf{x}_n \in \mathcal{D}$, as well as validation data in section 4.4.

D.1 Hessian Eigenvalue Estimation

The power method detailed in section D can be used to estimate the largest eigenvalue of the noise covariance matrix, as well as the Hessian. Importantly, for large networks, direct computation of any of the two matrices is infeasible due to the large number of parameters. Instead, we use efficient Jacobian-vector products for estimating the noise covariance (which entails accumulating the true gradient $\mathbb{E}_{\xi} \nabla_{\theta} \mathcal{L}$ at each iteration of the algorithm. For the Hessian matrix, Jacobian-vector products can be turned into Hessian-vector products using Pearlmutter's trick (Pearlmutter, 1994).

D.2 Hessian Trace Estimation

To estimate the Hessian trace in Figure 2, we use Hutchinson's algorithm (Hutchinson, 1990), which provides an unbiased estimator of the trace. At each iteration t , the algorithm generates a set of V random test vectors, $\mathbf{v}_n \in \mathbb{R}^p$ with zero mean $\mathbb{E} \mathbf{v}_n = \frac{1}{p} \sum_{i=1}^p v_n^i = 0$ and variance $\mathbb{E} [\mathbf{v}_n \mathbf{v}_n^T] = I_p$, by sampling each \mathbf{v}_n from the Rademacher distribution. At iteration t , the algorithm computes $\text{tr}_t = \frac{1}{V} \sum_{n=1}^V \mathbf{v}_n^T H \mathbf{v}_n$, where H is the expected loss Hessian.

Notably, the trace is obtained by computing $\frac{1}{V} \sum_{i=1}^p \mathbf{v}_n^T H \mathbf{v}_n = \text{tr} (\mathbf{v}_n^T H \mathbf{v}_n)$, where the Hessian is never instantiated and is implicitly computed via Hessian-vector products (Pearlmutter, 1994). In our work, we estimate the trace using $V = 100$ test vectors.

E Generating Random Validation Data

To generate random validation data for the experiments reported in Figure 8, we define several distributions over RGB pixels, and sample each pixel independently. We consider the following distributions:

- $\mathbf{x}_n \sim \mathcal{U}([\mu_{\text{CIFAR}} - \sigma_{\text{CIFAR}}, \mu_{\text{CIFAR}} + \sigma_{\text{CIFAR}}])$ pixel-wise
- $\mathbf{x}_n \sim \mathcal{N}([\mu_{\text{CIFAR}}, \mathcal{I}_3 \sigma_{\text{CIFAR}}])$ pixel-wise
- $\mathbf{x}_n \sim \mathcal{U}(S_{d-1})$ (pixel-wise) hypersphere
- $\mathbf{x}_n + \epsilon_n$, with ϵ strong random jitter

where μ_{CIFAR} and σ_{CIFAR} respectively denote the per-channel mean and standard deviation computed on the CIFAR-10 training set. For each distribution, we generate a validation set of 50k i.i.d. samples, and probe networks trained on the standard CIFAR-10 with 20% corrupted labels.

For reference, we also plot the empirical Lipschitz estimated on the CIFAR-10 train and test split. For both out-of-sample and in-sample validation datasets, it can be observed how the empirical Lipschitz remains bounded, and closely follows the double descent trend for the test error (c.f.r. Figure 1). Remarkably, the empirical Lipschitz on random validation data closely matches the one estimated on the training set, supporting the hypothesis of globally bounded function complexity.

F Proofs

In this section, we provide proofs for the formal statements presented in section 3. We begin by deriving results on boundedness of model function input-space gradients via parameter-space gradients. Then, we prove results of section 3.4, which rely on a recently developed noise model for discrete-step SGD.

F.1 Duality of Linear Layers

We begin by providing a general form of Theorem 1, generalizing the result of Ma & Ying (2021).

Theorem 1. *Let \mathbf{f} denote a neural network with a least one hidden layer, with $\|\boldsymbol{\theta}^1\| > 0$ and arbitrary weights $\boldsymbol{\theta}^2, \dots, \boldsymbol{\theta}^L$. Let $x_{\min} := \min_{\mathbf{x}_n \in \mathcal{D}} \|\mathbf{x}_n\|_2$. Then, parameter-space gradients bound input-space gradients of \mathbf{f} from above:*

$$\frac{x_{\min}^2}{\|\boldsymbol{\theta}^1\|_2^2} \mathbb{E}_{\mathcal{D}} \|\nabla_{\mathbf{x}} \mathbf{f}\|_2^2 \leq \mathbb{E}_{\mathcal{D}} \|\nabla_{\boldsymbol{\theta}} \mathbf{f}\|_2^2. \quad (3)$$

Proof. We recall that, by duality of inputs and weights in linear transformations, the partial derivatives $\frac{\partial}{\partial \mathbf{x}^{\ell-1}}$ and $\frac{\partial}{\partial \boldsymbol{\theta}^{\ell}}$ of any layer of the form $\mathbf{x}^{\ell} = \phi(\boldsymbol{\theta}^{\ell} \mathbf{x}^{\ell-1})$ are tied by the relation

$$\frac{\partial \mathbf{x}^{\ell}}{\partial \mathbf{x}^{\ell-1}} \mathbf{x}^{\ell-1T} = \boldsymbol{\theta}^{\ell T} \frac{\partial \mathbf{x}^{\ell}}{\partial \boldsymbol{\theta}^{\ell}} \quad (13)$$

Let $\mathbf{f} : \mathbb{R}^d \times \mathbb{R}^p \rightarrow \mathbb{R}^K$ be an arbitrary function composing linear layers with (optional) nonlinearities $\phi : \mathbb{R} \rightarrow \mathbb{R}$, that are differentiable a.e. Furthermore, let $\mathbb{R}^{d_{\ell}}$ denote the codomain of layer ℓ , i.e. $\mathbf{x}^{\ell} \in \mathbb{R}^{d_{\ell}}$.

Then, by the chain rule, for any layer ℓ , $\frac{\partial \mathbf{f}}{\partial \mathbf{x}^{\ell-1}} = \boldsymbol{\theta}^{\ell T} \frac{\partial \mathbf{f}}{\partial (\boldsymbol{\theta}^{\ell} \mathbf{x}^{\ell-1})}$. At the same time, $\frac{\partial \mathbf{f}}{\partial \boldsymbol{\theta}^{\ell}} = \frac{\partial \mathbf{f}}{\partial (\boldsymbol{\theta}^{\ell} \mathbf{x}^{\ell-1})} \mathbf{x}^{\ell-1T}$. Combining the two equations gives

$$\begin{aligned} \frac{\partial \mathbf{f}}{\partial \mathbf{x}^{\ell-1}} \mathbf{x}^{\ell-1T} &= \boldsymbol{\theta}^{\ell T} \frac{\partial \mathbf{f}}{\partial \boldsymbol{\theta}^{\ell}} \\ \left\| \frac{\partial \mathbf{f}}{\partial \mathbf{x}^{\ell-1}} \mathbf{x}^{\ell-1T} \right\| &= \left\| \boldsymbol{\theta}^{\ell T} \frac{\partial \mathbf{f}}{\partial \boldsymbol{\theta}^{\ell}} \right\| \\ \frac{1}{\|\mathbf{x}\|} \left\| \frac{\partial \mathbf{f}}{\partial \mathbf{x}^{\ell-1}} \mathbf{x}^{\ell-1T} \right\| &= \frac{1}{\|\mathbf{x}\|} \left\| \boldsymbol{\theta}^{\ell T} \frac{\partial \mathbf{f}}{\partial \boldsymbol{\theta}^{\ell}} \right\| \quad \text{for } \mathbf{x} \in \mathbb{R}^{d_{\ell}} \setminus \{\mathbf{0}\} \\ \sup_{\mathbf{x}: \|\mathbf{x}\| \neq 0} \frac{1}{\|\mathbf{x}\|} \left\| \frac{\partial \mathbf{f}}{\partial \mathbf{x}^{\ell-1}} \mathbf{x}^{\ell-1T} \right\| &= \sup_{\mathbf{x}: \|\mathbf{x}\| \neq 0} \frac{1}{\|\mathbf{x}\|} \left\| \boldsymbol{\theta}^{\ell T} \frac{\partial \mathbf{f}}{\partial \boldsymbol{\theta}^{\ell}} \right\| \\ \left\| \frac{\partial \mathbf{f}}{\partial \mathbf{x}^{\ell-1}} \right\|_2 &= \sup_{\mathbf{x}: \|\mathbf{x}\| \neq 0} \frac{1}{\|\mathbf{x}\|} \left\| \boldsymbol{\theta}^{\ell T} \frac{\partial \mathbf{f}}{\partial \boldsymbol{\theta}^{\ell}} \right\| \end{aligned} \quad (14)$$

Evaluating the equation on a set of data points $\{\mathbf{x}_1, \dots, \mathbf{x}_N\} \subset \mathbb{R}^d$, with corresponding activations $\{\mathbf{x}_1^{\ell}, \dots, \mathbf{x}_N^{\ell}\} \subset \mathbb{R}^{d_{\ell}}$ yields:

$$\left\| \frac{\partial \mathbf{f}}{\partial \mathbf{x}^{\ell-1}} \right\|_2 = \frac{1}{\min_n \|\mathbf{x}_n^{\ell}\|} \left\| \boldsymbol{\theta}^{\ell T} \frac{\partial \mathbf{f}}{\partial \boldsymbol{\theta}^{\ell}} \right\| \leq \frac{\|\boldsymbol{\theta}^{\ell T}\|}{\min_n \|\mathbf{x}_n^{\ell}\|} \left\| \frac{\partial \mathbf{f}}{\partial \boldsymbol{\theta}^{\ell}} \right\| \quad (15)$$

Particularly, given a finite dataset \mathcal{D} , applying Equation 15 to the gradients $\nabla_{\mathbf{x}} \mathbf{f}$ and $\nabla_{\boldsymbol{\theta}} \mathbf{f}$, and taking the expectation over \mathcal{D} on both sides concludes the proof. \square

We emphasize that, while the bound was already observed in Ma & Ying (2021), the authors propose to bound $\nabla_{\boldsymbol{\theta}} \mathbf{f}$ via a uniform bound that linearly depends on model size, and thus cannot capture double descent. In this work, we improve upon their bounds, by explicitly studying Equation 4 in connection to parameter-space dynamics.

F.2 Extension to loss functions

For losses $\mathcal{L} : \mathbb{R}^p \times \mathbb{R}^d \times \mathcal{Y} \rightarrow \mathbb{R}^+$ of the exponential family (De Brebisson & Vincent, 2016) like mean squared error and cross entropy, the following corollary holds.

Corollary 1. *Consider the composition of a loss function \mathcal{L} with a neural network \mathbf{f} with a least one hidden layer, with $\|\theta^1\| > 0$ and arbitrary weights $\theta^2, \dots, \theta^L$. Then,*

$$\frac{x_{\min}^2}{\|\theta^1\|_2^2} \mathbb{E}_{\mathcal{D}} \|\nabla_{\mathbf{x}} \mathcal{L}\|_2^2 \leq \mathbb{E}_{\mathcal{D}} \|\nabla_{\theta} \mathcal{L}\|_2^2. \quad (4)$$

Proof. For each sample (\mathbf{x}_n, y_n) , the gradient $\frac{\partial \mathcal{L}}{\partial \mathbf{f}}$ takes the form $\mathbf{p}_n - \mathbf{e}_{y_n}$. For crossentropy, \mathbf{p}_n denotes the softmax normalized logits, and \mathbf{e}_{y_n} the one-hot encoded label y_n . For mean squared error, $\mathbf{p}_n = \mathbf{f}_{\theta}(\mathbf{x}_n)$.

When composing the loss with a model \mathbf{f} , we have

$$\begin{aligned} \nabla_{\theta}(\mathcal{L} \circ \mathbf{f}) &= (\mathbf{p}_n - \mathbf{e}_{y_n}) \nabla_{\theta} \mathbf{f} \\ \nabla_{\mathbf{x}}(\mathcal{L} \circ \mathbf{f}) &= (\mathbf{p}_n - \mathbf{e}_{y_n}) \nabla_{\mathbf{x}} \mathbf{f} \end{aligned} \quad (16)$$

Applying Theorem 1 trivially concludes the proof. \square

Importantly, the term $\|\mathbf{p}_n - \mathbf{e}_{y_n}\|$ is inversely proportional to the model confidence (Brier, 1950) $\sigma = 1 - \frac{1}{N} \sum_{n=1}^N \|\mathbf{p}_n - \mathbf{e}_{y_n}\|$, which generally saturates for large models, typically yielding high confidence predictions at convergence. In section C.1 we empirically study how the quantity is affected by model size, to understand its impact on the bounds presented throughout section 3.

Next, we provide proofs for section 3.4.

F.3 Connection to Parameter-Space Curvature

In this section, we prove formal statements connecting Theorem 1 to the dynamics of SGD in proximity of a critical point θ^* . For our proofs, we use the mean square error $\mathbb{E}_{\mathcal{D}} \mathcal{L} = \frac{1}{2N} \sum_{n=1}^N (f_{\theta}(\mathbf{x}_n) - y_n)^2$, and adopt a recent model of stochastic noise proposed by Liu et al. (2021). The crux of the proof of Theorem 2 is bounding $\mathbb{E}_{\mathcal{D}} \|\nabla_{\theta} \mathcal{L}\|$ with $\text{tr}(H)$, which we can later connect to the noise uncentered covariance S .

Theorem 2. *Let θ^* be a critical point for the loss $\mathcal{L}(\theta, \mathbf{x}, y)$ on \mathcal{D} . Let \mathbf{f}_{θ} denote a neural network with at least one hidden layer, with $\|\theta^1\| > 0$. Then,*

$$\frac{x_{\min}^2}{\|\theta^1\|_2^2} \mathbb{E}_{\mathcal{D}} \|\nabla_{\mathbf{x}} \mathcal{L}\|_2^2 \leq 2\mathcal{L}_{\max}(\theta) \Delta(\mathcal{L}(\theta)) + o(\mathcal{L}(\theta)) \quad (6)$$

with $\Delta(\mathcal{L}(\theta)) := \text{tr}(H)$ denoting the Laplace operator; $H := \mathbb{E}_{\mathcal{D}} [\frac{\partial^2 \mathcal{L}}{\partial \theta \partial \theta^T}]$ denoting the expected parameter-space Hessian of \mathcal{L} , and $\mathcal{L}_{\max}(\theta) := \max_{(\mathbf{x}_n, y_n) \in \mathcal{D}} \mathcal{L}(\theta, \mathbf{x}_n, y_n)$.

Proof. The proof is broken down in two parts. First, we write out explicitly the expected Hessian H of \mathcal{L} .

$$H = \frac{1}{N} \sum_{n=1}^N \frac{\partial^2}{\partial \theta \partial \theta^T} \mathcal{L}_n = \frac{1}{N} \sum_{n=1}^N \mathcal{L}_n'' \nabla_{\theta} \mathbf{f}_n \nabla_{\theta} \mathbf{f}_n^T + \frac{1}{N} \sum_{n=1}^N \mathcal{L}_n' \frac{\partial^2}{\partial \theta \partial \theta^T} \mathbf{f}_n \quad (17)$$

with $\mathbf{f}_n := \mathbf{f}(\mathbf{x}_n, \theta)$, for $n = 1, \dots, N$.

By noting that $\mathcal{L}_n'' = 1, \forall n$, and that $\mathcal{L}_n' \propto \mathcal{L}_n \rightarrow 0$ as $\|\theta - \theta^*\|^2 \rightarrow 0$ for interpolating models, the expected loss Hessian amounts to the cross term

$$H = \frac{1}{N} \sum_{n=1}^N \nabla_{\theta} \mathbf{f}_n \nabla_{\theta} \mathbf{f}_n^T + \mathcal{O}(\mathcal{L}) \quad (18)$$

Next, we connect $\|\nabla_{\theta}\mathcal{L}\|_2^2$ to H . We note that $\frac{1}{N} \sum_{n=1}^N \nabla_{\theta}\mathcal{L} = \mathcal{L}'_n \nabla_{\theta}\mathbf{f}_n$. Then, by definition of norm:

$$\begin{aligned}
 \mathbb{E}_{\mathcal{D}} \|\nabla_{\theta}\mathcal{L}\|_2^2 &= \mathbb{E}_{\mathcal{D}} \nabla_{\theta}\mathcal{L}^T \nabla_{\theta}\mathcal{L} \\
 &= \mathbb{E}_{\mathcal{D}} \text{tr}(\nabla_{\theta}\mathcal{L} \nabla_{\theta}\mathcal{L}^T) \\
 &= \text{tr}\left(\frac{1}{N} \sum_{n=1}^N [\mathcal{L}'_n^2 \nabla_{\theta}\mathbf{f}_n \nabla_{\theta}\mathbf{f}_n^T]\right) \\
 &\leq 2 \left(\max_{1 \leq n \leq N} \mathcal{L}'_n^2\right) \left(\text{tr}\left(\frac{1}{N} \sum_{n=1}^N \nabla_{\theta}\mathbf{f}_n \nabla_{\theta}\mathbf{f}_n^T\right)\right) \\
 &= 2\mathcal{L}_{\max}(\theta) \text{tr}(H) \\
 &= 2\mathcal{L}_{\max}(\theta) \Delta\mathcal{L}(\theta)
 \end{aligned} \tag{19}$$

□

Having built a connection between $\nabla_{\theta}\mathcal{L}$ and H , we can prove Corollary 2.

Corollary 2. *Let θ^* be a critical point for the loss $\mathcal{L}(\theta, \mathbf{x}, y)$ on \mathcal{D} . Let \mathbf{f}_{θ} denote a neural network with at least one hidden layer, with $\|\theta^1\| > 0$. Then,*

$$\frac{x_{\min}^2}{\|\theta^1\|_2^2} \mathbb{E}_{\mathcal{D}} \|\nabla_{\mathbf{x}}\mathcal{L}\|_2^2 \leq \text{tr}(S) + o(\mathcal{L}(\theta)) \tag{9}$$

with $S = C + \frac{1}{B} \mathbb{E}_{\mathcal{D}} [\nabla_{\theta}\mathcal{L}(\theta)] \mathbb{E}_{\mathcal{D}} [\nabla_{\theta}\mathcal{L}(\theta)]^T$ denoting the gradient uncentered covariance.

Proof.

$$\begin{aligned}
 \mathbb{E}_{\mathcal{D}} \|\nabla_{\theta}\mathcal{L}\|_2^2 &= \mathbb{E}_{\mathcal{D}} \nabla_{\theta}\mathcal{L}^T \nabla_{\theta}\mathcal{L} \\
 &= \mathbb{E}_{\mathcal{D}} \text{tr}(\nabla_{\theta}\mathcal{L} \nabla_{\theta}\mathcal{L}^T) \\
 &= \text{tr}\left(\frac{1}{N} \sum_{n=1}^N [\mathcal{L}'_n^2 \nabla_{\theta}\mathbf{f}_n \nabla_{\theta}\mathbf{f}_n^T]\right) \\
 &= \text{tr}(S)
 \end{aligned} \tag{20}$$

□

F.4 Stability of the bound

We conclude this section by proving Corollary 3, which connects the bound to the training hyperparameters via the approximation error $\mathcal{L}(\theta) - \mathcal{L}(\theta^*)$. We use the following lemma, providing a closed form for the approximation error of SGD with finite learning rate η .

Lemma 1. *Theorem 5 in (Liu et al. (2021)) The training error for SGD with momentum μ , batch size B , and learning rate η is given by*

$$\mathcal{L}(\theta) = \frac{\eta}{4(1-\mu)} \text{tr} \left[\left[I_p - \frac{\eta}{2(1+\mu)} H \right]^{-1} C \right] \tag{21}$$

Combining the above lemma with Theorem 2 proves Corollary 3, where the trace in Equation 21 is replaced by the maximum eigenvalue λ_{\max} to account for $\mathcal{L}_{\max}(\theta)$ in Equation 6.

Corollary 3. *Let θ^* be a critical point for the loss $\mathcal{L}(\theta, \mathbf{x}, y)$ on \mathcal{D} . Let \mathbf{f}_{θ} denote a neural network with at least one hidden layer, with $\|\theta^1\| > 0$. Then,*

$$\begin{aligned}
 \frac{x_{\min}^2}{\|\theta^1\|_2^2} \mathbb{E}_{\mathcal{D}} \|\nabla_{\mathbf{x}}\mathcal{L}\|_2^2 &\leq o(\mathcal{L}(\theta)) + \\
 &\quad \frac{\eta}{2(1-\mu)} \lambda_{\max} \left[\left(I_p - \frac{\eta}{2(1+\mu)} H \right)^{-1} C \right] \text{tr}(H)
 \end{aligned} \tag{10}$$